IEEE Access
Multidisciplinary | Rapid Review | Open Access Journal

Received January 14, 2020, accepted January 26, 2020, date of publication January 29, 2020, date of current version February 6, 2020.

Digital Object Identifier 10.1109/ACCESS.2020.2970204

Corrosion Depth Inversion Method Based on the Lift-Off Effect of the Capacitive Imaging (CI) Technique

XIAOKANG YIN, ZHEN LI, XIN'AN YUAN, WEI LI, (Member, IEEE), AND GUOMING CHEN
Centre for Offshore Engineering and Safety Technology, China University of Petroleum (East China), Qingdao 266580, China

Corresponding author: Zhen Li (lizhenndt@163.com)

This work was supported in part by the National Natural Science Foundation of China under Grant 51675536 and Grant 51574276, in part by the Fundamental Research Funds for the Central Universities under Grant 18CX02084A, in part by the Postgraduate Innovation Project of the China University of Petroleum under Grant YCX2019057, in part by the National Postdoctoral Program for Innovative Talents under Grant BX20190386, and in part by the China Postdoctoral Science Foundation Project under Grant 2019M662461.

ABSTRACT As a new Non-destructive Evaluation (NDE) technique, capacitive imaging (CI) has been used to detect defects in oil pipelines, composite sucker rods and storage tanks in recent years. When a CI sensor is used to detect corrosion defect on a conducting surface with or without an insulation layer, the depth information of corrosion defect is difficult to acquire due to the non-linearity of the probing field. This paper proposed a corrosion depth inversion method based on the lift-off effect of the CI technique. The proposed depth inversion method, which includes three steps, namely establishing the lift-off curve, obtaining the scan curve and fitting inversion, are introduced and evaluated. In the FE simulations, the error rates of the inversion depths are less than 1.20%. CI experiments were carried out to acquire the depth information of a step shape specimen using the CI experimental system and the proposed corrosion depth inversion method. The results show that the depth inversion method can meet the need of obtaining the actual depth information with the error rates of the inversion depths being less than 10.00%. A CI experiment on a machined and corroded specimen was carried out to further demonstrate the feasibility of the proposed inversion method for corrosion defects with different depths. Both results from FE models and experiments indicate that the proposed method is promising to achieve the quantitative NDE of the Corrosion Under Insulation (CUI).

INDEX TERMS Capacitive imaging, corrosion defect, depth inversion, lift-off effect, insulation layer.

I. INTRODUCTION

Corrosion, which is the most common type of defects on metals, affects the operation reliability of the metal structure and component and can cause huge losses [1]–[3]. For metallic oil and gas pipelines with insulation layers, water and natural minerals can intrude into the insulation layer and have oxidation and electrochemical reaction with the metal surface of the pipeline. This will result in corrosion under insulation (CUI) and may lead to major safety accidents [4]. If the depth information of corrosion defect is accurately obtained, the condition of the pipeline can be properly assessed, and a suitable maintenance scheme can be adopted to ensure the safe operation of the pipeline. How to effectively detect and acquire the depths information of surface corrosion defects on conducting specimens with and without insulation layer has been extensively studied in the Non-destructive Evaluation (NDE) field [5]–[8]. There are many kinds of detection methods (Ultrasonic Testing (UT) [9], Eddy Current [10], Magnetic Flux Leakage (MFL) [11], X-ray [12]) to solve this problem. However, the insulation layer needs to be removed in many cases, which will significantly increase the inspection cost [9], [13].

Capacitive imaging (CI) has been used for the inspection of oil pipelines, composite sucker rods and storage tanks in recent years [14]. It has many advantages, such as non-contact, coupling agent free, real-time and intuitive detection results, cost effective and easy to implement [15]. In theory, the CI technique can not only detect surface corrosion defects of the conducting specimen without an insulation layer but also detect surface corrosion defects of the conducting specimen through a relatively thick (up to 100 mm) insulation

The associate editor coordinating the review of this manuscript and approving it for publication was Wuliang Yin.

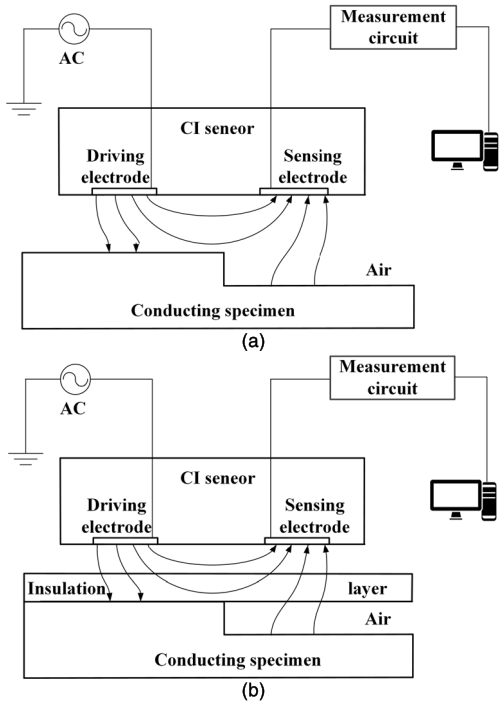

FIGURE 1. Detection principle of the CI technique: (a) CI sensor inspecting a conducting specimen without insulation layer. (b) CI sensor inspecting a conducting specimen covered by an insulation layer.

layer [16]. The principle of CI technique for defect detection is shown in Fig 1. An AC voltage is applied to the driving electrode of a CI sensor, and the sensing electrode of the CI sensor is connected to a measurement circuit. Because the frequency of this AC voltage is usually below 100 kHz, the electric field between these two electrodes of CI sensor can be considered as a quasi-static fringing electric field [17]. When a CI sensor is used to inspect the conducting specimen without insulation layer, as shown in Fig 1(a), if a corrosion defect is presented (shown as a step shape metal loss in Fig. 1(a)), the distribution of the probing field between the driving and sensing electrode will be altered. This change of the probing field will cause a charge variation on the sensing electrode of CI sensor. The charge variation can be measured and used to reflect depth information of the corrosion defects of the conducting specimen without insulation layer. For the case in which an insulation layer is presented, as shown in Fig 1(b), the quasi-static fringing electric field will penetrate through the insulation layer and be influenced by the corrosion defects (metal loss) on the upper surface of the conducting specimen. This will again cause charge variation on the sensing electrode, which can also be measured and used to reflect depth information of the corrosion defects under insulation.

Previous attempts using the CI technique were focused on detecting the presence of the defects, and how to quantify the detected defect remains unanswered. Due to the non-linearity of the quasi-static fringing electric field of CI sensor, it is difficult to acquire the surface corrosion depth information of the conducting specimen. To solve this problem, this work

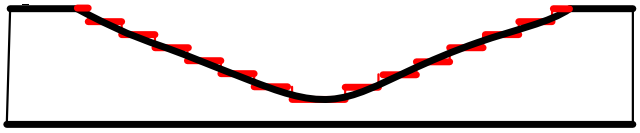

FIGURE 2. Corrosion defect conversion diagram.

proposes a corrosion depth inversion method based on the lift-off effect of the CI technique. The method was briefly introduced in Section 2. Finite element (FE) models were constructed in COMSOL^{TM}, and the proposed depth inversion method was implemented based on the FE modes in Section 3. In Section 4, depth inversions in CI experiments were also carried out on specimens with artificial metal losses and corrosions. The discussions and conclusions are presented in Section 5.

II. THE CORROSION DEPTH INVERSION METHOD

Real corrosion defects are often of irregular depth profiles, which increases the difficulty of corrosion depth inversion. To simplify this problem, the profile of a corrosion detect (the black lines in Fig 2) can be approximated by a set of regular metal losses characterized by small horizontal and vertical lines (the red lines in Fig 2), and the depth information of the whole defect can be summarized by the depth information of each small regular segment.

To achieve the depth inversion of each regular segment, an inversion method based on the lift-off effect of CI technique is proposed. The basic idea of this corrosion depth inversion method is that the depth of surface corrosion defect is equivalent to the change of the lift-off. If the lift-off to the conducting surface can be inferred from the measured data, so can the corrosion depth. The equivalent schematic diagram of the corrosion depth inversion method is shown in Fig 3. For the inspection of conducting specimens without insulation layer, as shown in Fig 3(a), the corrosion depth (metal loss) is equal to the difference between lift-off #2 and lift-off #1. Both lift-off #1 and #2 are the distances between the sensor surface and the conducting surface. For the inspection of conducting specimens covered by an insulation layer, as shown in Fig 3(b), the corrosion depth is equal to the distance between the bottom surface of the insulation layer and the top surface of the conductor (also referred to as ''lift-off'' for such cases in the remaining part of this work).

The proposed corrosion depth inversion method mainly contains three steps, namely establishing the lift-off curve (Step I), obtaining the scan curve (Step II) and fitting inversion (Step III), as shown in Fig. 4. Step I is to establish a lift-off curve, which is the non-linear relationship between the measured values and lift-offs. Step II is to obtain the scan curve. In this step, the CI sensor is used to scan the specimen at a fixed lift-off, and the relationship between the measured values and line-scanning positions can be obtained. Step III is fitting inversion. In this step, the measured values in the scan curve are searched in the lift-off curve, and the relationship between lift-off (equivalent to the depth of metal

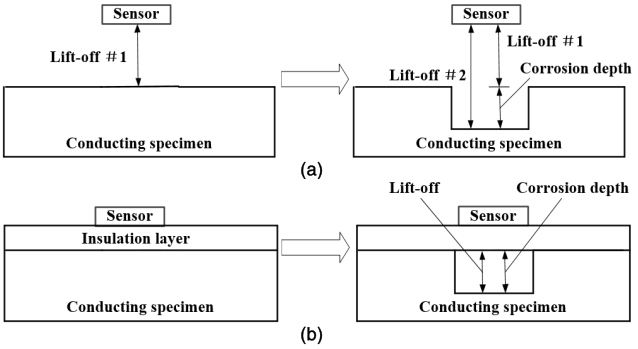

FIGURE 3. Equivalent schematic diagram: (a) A conducting specimen without insulation layer. (b) A conducting specimen covered by an insulation layer.

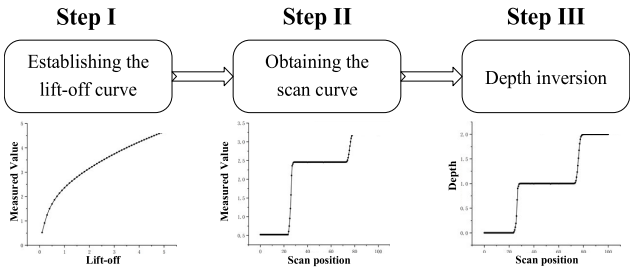

FIGURE 4. Flow chart of the corrosion depth inversion method.

loss/corrosion) and line-scanning position can be obtained. Different fitting methods, including polynomial fitting, least square method and neural network algorithms can be used. After these three steps, the depth information of surface corrosion defect of the conducting specimen can be obtained. In practice, the lift-off curve can be established in advance according to the inspection conditions (i.e. types of targets under test, experimental conditions, etc.), and the later two steps can be done during the scanning process, leading to a real-time inversion for the corrosion depth. The non-linearity of the probing field was reflected in the lift-off curve and requires no further treatment.

III. SIMULATION ANALYSIS OF THE CI SENSOR DETECTING SURFACE CORROSION DEFECTS

A. THE FE MODEL

It is well known that for static electric field, the electric field lines and the equipotential lines are perpendicular to each other [16]. If there is a defect in the quasi-static fringing electric field, both the electric field lines and the equipotential lines will be distorted [17]. For a better illustration, equipotential lines were used to demonstrate the electric field distribution. According to equations (1) and (2), the potential distribution can be obtained from FE models [18], [19].

$$E = -\nabla\varphi \tag{1}$$

$$\nabla\left(\varepsilon_0\varepsilon_r\nabla\varphi\right) = 0 \tag{2}$$

where, E denotes the electric field, φ denotes the electric potential distribution, ε_o denotes the electric constant or the permittivity of a vacuum, and ε_r denotes the relative permittivity.

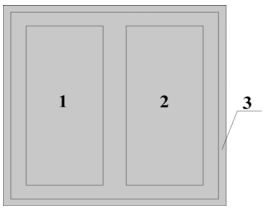

FIGURE 5. A CI sensor with rectangular electrodes.

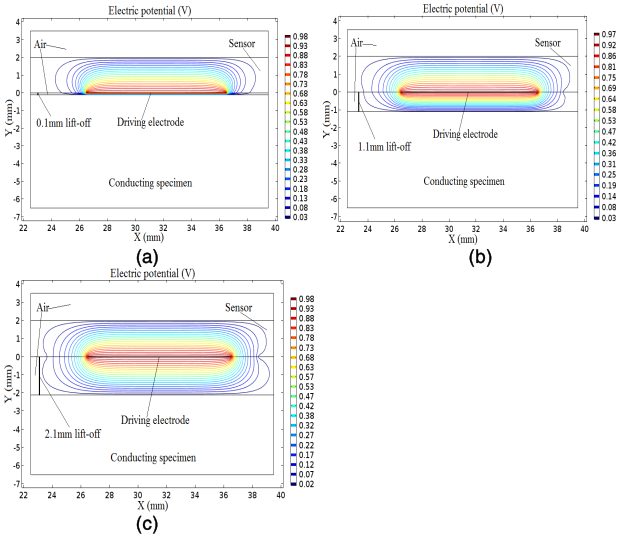

FIGURE 6. Equipotential line diagrams of a CI sensor inspecting a conducting specimen without an insulation layer: (a) 0.1 mm lift-off. (b) 1.1 mm lift-off. (c) 2.1 mm lift-off.

To demonstrate the feasibility of using a CI sensor to detect surface corrosion defects, FE models were constructed in COMSOL^{TM}. A CI sensor with rectangular electrodes (shown in Fig 5) was used. The CI sensor consists of a driving electrode (No.1) and a sensing electrode (No.2). The center distance between these two electrodes (No.1 and No.2) was 13 mm. To shield external stray capacitance, this CI sensor also has a surrounding shielding electrode (No.3). The total size of this CI sensor was 30 mm $\times$ 30 mm, and the two co-planar electrodes (No.1 and No.2) were both 10 mm $\times$ 23 mm.

The equipotential line diagrams of a CI sensor on a conducting specimen (aluminium plate) without an insulation layer are shown in Fig 6. To avoid galvanic contact between the electrodes and the specimen, the minimal lift-off between the CI sensor and the conducting specimen cannot be zero, and was set to be 0.1mm in this case. In Fig 6(a), (b) and (c), the lift-offs between the CI sensor and the conducting specimen were 0.1 mm, 1.1 mm and 2.1 mm respectively. Comparing Fig 6(a), (b) and (c), it can be seen that the equipotential lines would extend to the surface of the conducting specimen with increased depths (lift-offs between the CI sensor and the conducting specimen) in all three models. The changes in the equipotential lines show that the CI sensor could response to different lift-offs which is equivalent to corrosion depths.

The equipotential line diagrams of a CI sensor on a conducting specimen covered by an insulation layer

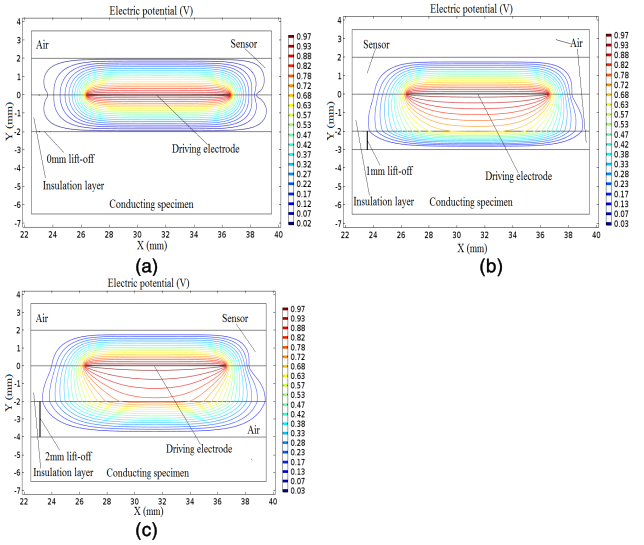

FIGURE 7. Equipotential line diagrams of a CI sensor inspecting a conducting specimen with an insulation layer: (a) 0 mm lift-off. (b) 1 mm lift-off. (c) 2 mm lift-off.

(polymethyl methacrylate, PMMA) are shown in Fig 7. Because there is an insulation layer between the CI sensor and the conducting specimen, the minimal lift-off between the insulation layer and the conducting specimen can be zero. In Fig 7(a), (b) and (c), the lift-offs between the insulation layer and the conducting specimen were 0 mm, 1 mm and 2 mm respectively. Comparing Fig 7(a), (b) and (c), it can be seen that the equipotential lines would extend to the surface of the conducting specimen with increased depths) of corrosion defects (lift-offs between the insulation layer and the conducting specimen. The changes in the equipotential lines show that the CI sensor could response to different lift-offs which is equivalent to corrosion depths under insulation.

B. DEPTH INVERSION FOR A SPECIMEN WITHOUT INSULATION LAYER IN FE MODELS

As mentioned in Section 2, the depth inversion method for surface corrosion defects comprises three steps, namely establishing lift-off curve, obtaining scan curve and fitting inversion. As shown in Fig 8(a), the baseline was located on the surface of the conducting specimen, and the lift-off was the distance between the CI sensor and the baseline. The conducting specimen was of step shape and the depths of the second and third steps were1 mm and 2 mm. The first step of the depth inversion is to establish the lift-off curve. Simulated CI measurements were taken with increased lift-offs (from 0.1 mm to 5 mm at a 0.1mm increment), as shown in Fig 8(a). The cross-section of the FE model is shown in Fig 8(b). The obtained lift-off curve which contains 50 points, is shown in Fig 8(c). It can be seen that the capacitance values from the CI sensor rose monotonously with increased lift-offs, which enables the possibility for the depth inversion.

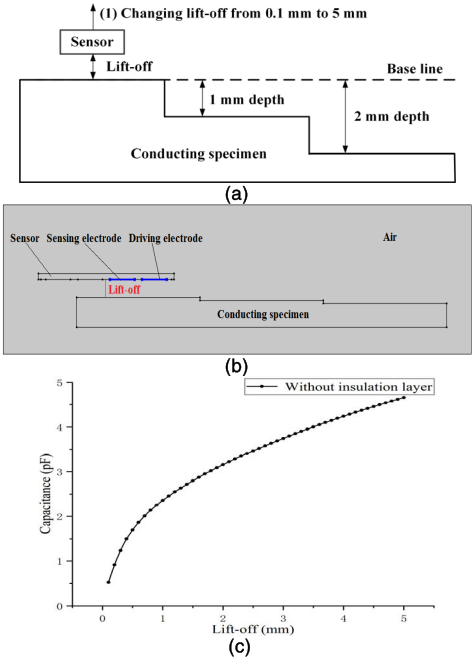

FIGURE 8. The first step of the corrosion depth inversion method: (a) schematic diagram. (b) Cross-section of the FE model (scan with increased lift-off). (c) The obtained lift-off curve.

The second step of the depth inversion is obtaining the scan curve. In this step, the CI sensor was used to inspect the conducting specimen along the scanning path at a 0.1 mm lift-off (shown in Fig 9(a)). A 0.1 mm lift-off instead of 0 mm (minimal lift-off) was chosen to avoid galvanic contact between the sensor and the conducting surface. Note that, this lift-off should be deducted from the inversion results. The cross-section of the FE model is shown in Fig 9(b). The length of the line-scanning detection was 100 mm, and the step-size for the line-scanning detection in the horizontal direction was 0.5 mm. The scan curve which contain 201 points is shown in Fig 9(c). It can be seen that the scan curve can only reflect the step shape of the corrosion defects, and the actual depth information remains unknown.

The third step of the depth inversion is fitting inversion. A fitting method using neural network was adopted to improve the inversion efficiency and accuracy. The number of data in the lift-off curve was too small (50 point), to train the neural network, it is thus necessary to increase the number of samples (points). Due to the monotonicity of the lift-off curve, an interpolation function can be used. The number of the data was increased to 491 after interpolation. A ten-layer neural network was trained with the interpolated lift-off dataset. The scan curve (in this case, a simulated line scan shown in Fig 9(c)) were then taken to the trained neural networks to obtain the inversion depths (shown in Fig 10). It was found that the inversion depth can reflect the actual depth information, which demonstrates the effectiveness of the depth inversion method of surface corrosion defects of the conducting specimen without an insulation layer.

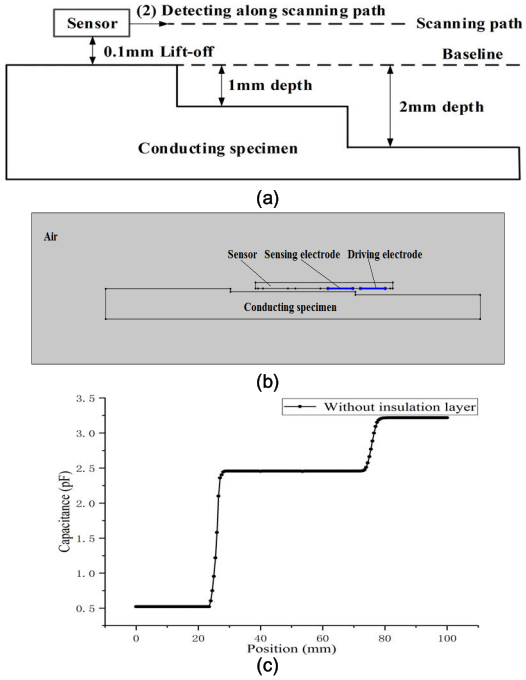

FIGURE 9. The first step of the corrosion depth inversion method: (a) Schematic diagram. (b) Cross-section of the FE model (scan with increased lift-off). (c) The obtained lift-off curve.

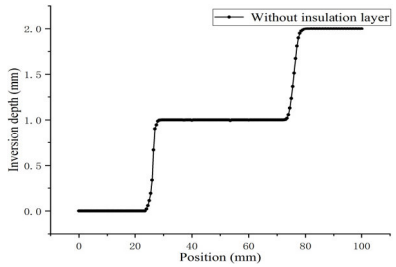

FIGURE 10. Inversion curve.

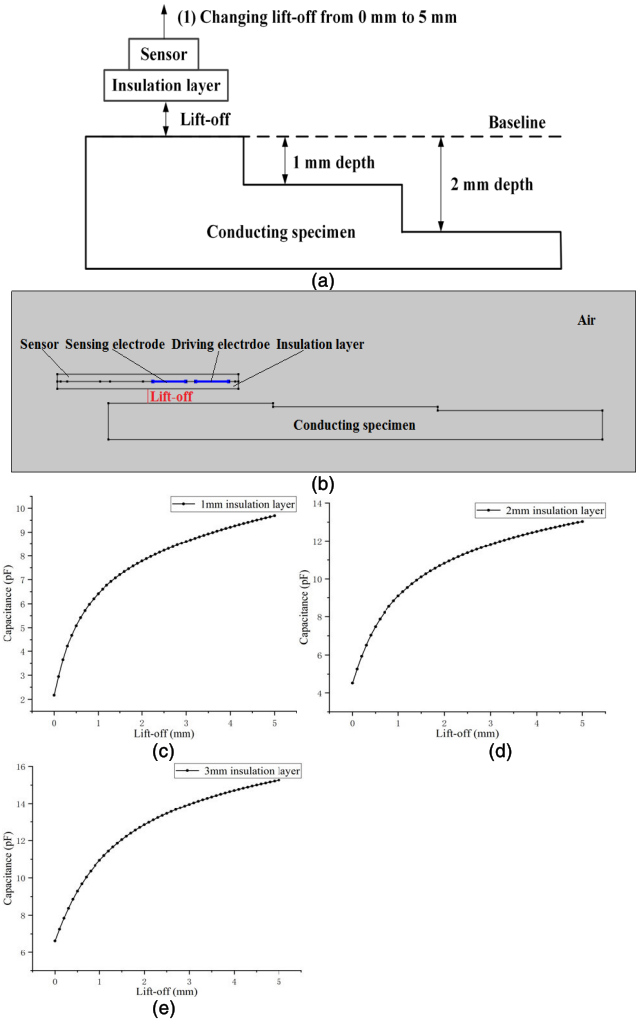

FIGURE 11. The first step of the corrosion depth inversion method: (a) Schematic diagram. (b) Cross-section of the FE model (scan with increased lift-off). (c) Lift-off curve for 1 mm insulation layer. (d) Obtained lift-off curve for 2 mm insulation layer. (e) Lift-off curve for 3 mm insulation layer.

C. DEPTH INVERSION FOR A SPECIMEN WITH AN INSULATION LAYER IN FE MODELS

Depth inversion for specimens with insulation layers was also implemented in FE models. The schematic diagram for establishing lift-off curve (Step I) is shown in Fig 11(a). The baseline was located on the surface of the conducting specimen, and the lift-off was the distance between the insulation layer and the baseline. The conducting specimen contained two corrosion defects (step shape metal losses) of different depths (1 mm and 2 mm). The cross-section of the FE model is shown in Fig 11(b). In the FE model, the CI sensor was attached to an insulation layer (PMMA). The lift-off curves for three insulation layers with different thicknesses (1 mm, 2 mm and 3 mm) were obtained and shown in Fig 11(c), (d) and (e).

The scan curves for the conducting specimen with different insulation layers (1 mm, 2 mm and 3 mm) at a minimal lift-off (shown in Fig 12(a)) were also obtained from FE models. Note that, in order to be in accordance with step I, the san was taken with the sensor in contact with the insulation layer. The cross-section of the FE model is shown in Fig 12(b). The length for each line scan was 100 mm, and the step-size scanning direction was 0.5 mm. The scan curves for the three insulation layers are shown in Fig 12(c), (d) and (e).

Similar to the case in Section 3.2, the fitting inversion was also done with the fitting method and the results are shown in Fig 13(a), (b) and (c). It can be seen that the inversion depths can reflect the actual depth information, which again demonstrates the effectiveness of the depth inversion method for specimen with an insulation layer.

The error rates for the depth inversion in FE models (both in Section 3.2 and 3.3) were calculated and shown in Table 1. The errors of the inversion depths were less than 0.002 mm and the error rates of the inversion depths were less than 1.20%, which proves the effectiveness of the depth inversion method in FE models.

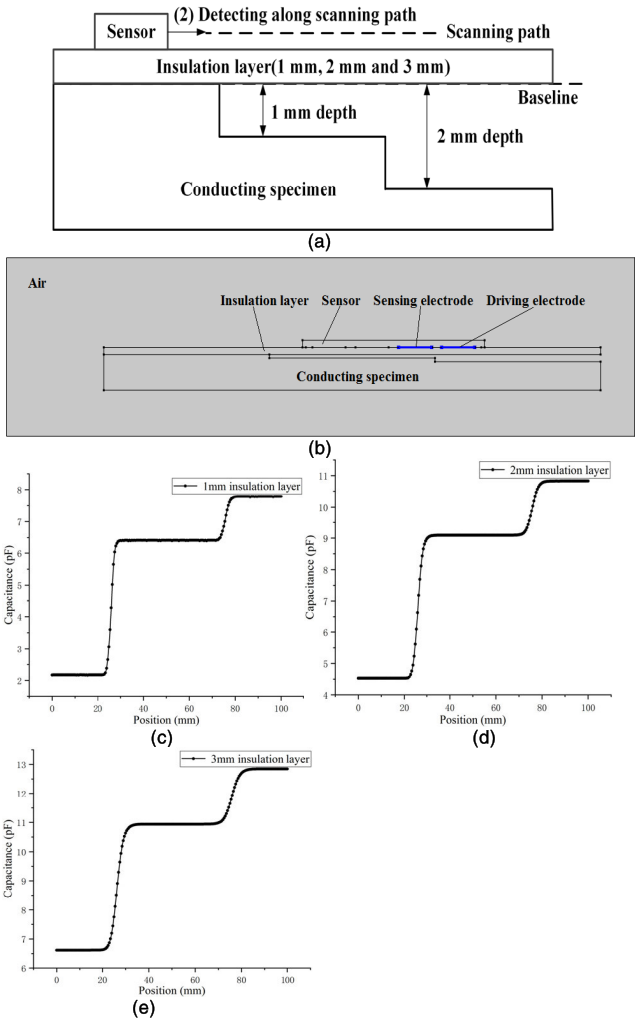

FIGURE 12. The second step of the corrosion depth inversion method: (a) Schematic diagram. (b Cross-section of the FE model (line-scanning). (c) Scan curve for 1 mm insulation layer. (d) Scan curve for 2 mm insulation layer. (e) Scan curve for 3 mm insulation layer.

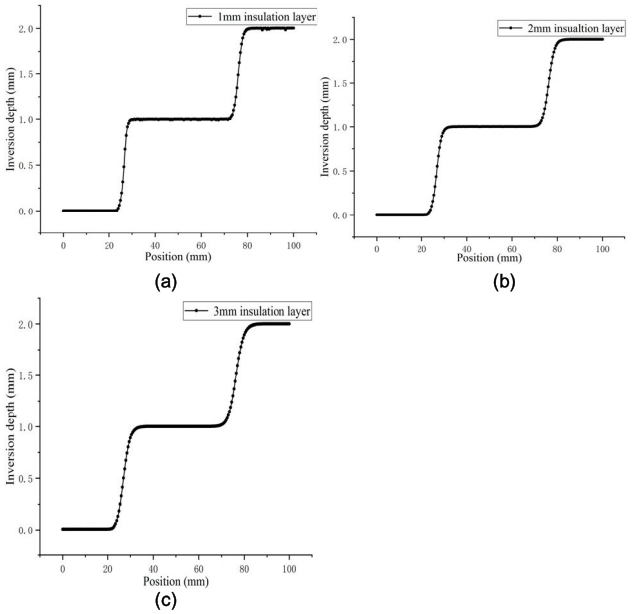

FIGURE 13. Inversion curves: (a) 1 mm insulation layer. (b) 2 mm insulation layer. (c) 3 mm insulation layer.

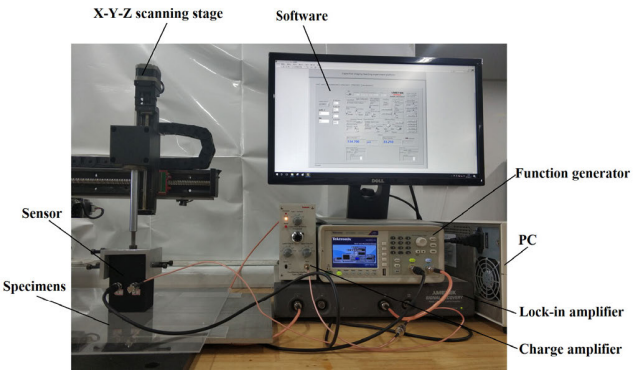

FIGURE 14. Picture of the experimental system.

TABLE 1. Error rates for depth inversion in FE models.

Depth of defect (mm)	Without insulation layer (mm)/ Error rate (%)	1 mm insulation layer (mm) /Error rate (%)	2 mm insulation layer (mm) /Error rate (%)	3 mm insulation layer (mm) /Error rate (%)
1	1.0002/ 0.20	0.9992/ 0.80	1.0012/ 1.20	1.0004/ 0.40
2	1.9995/ 0.25	2.0015/ 0.75	2.0002/ 0.10	2.0005/ 0.25

IV. EXPERIMENTAL VALIDATION

To validate the proposed inversion method in experiments, a CI experimental system was developed, as shown in Fig 14. This CI system consists of a CI sensor, a function generator, a charge amplifier, a lock-in amplifier, an X-Y-Z scanning stage, a PC with scan control and data acquisition software [20]. The function generator was used to generate a 10V Pk-Pk AC voltage, and the frequency of this voltage was 10 kHz [21]. A charge amplifier was used to convert the charge signal from the CI sensor into an AC voltage signal [22]. This AC voltage signal was then measured by the lock-in amplifier [23]. The X-Y-Z scanning stage was controlled and used to manipulate the CI sensor to establish the lift-off curves and obtain the scan curves.

A. DEPTH INVERSION FOR A SPECIMEN WITHOUT INSULATION LAYER IN EXPERIMENTS

As shown in Fig 15(a), a step shape conducting specimen (aluminium plate) was inspected in experiments. The two lower steps were to simulate surface corrosion defects. The sizes of the steps were 100 mm × 50 mm × 1 mm and 100 mm × 50 mm × 2 mm respectively. The first step of the depth inversion is to establish the lift-off curve, in which the

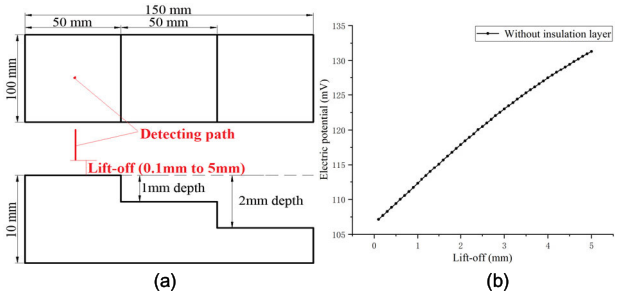

FIGURE 15. The first step of the corrosion depth inversion method: (a) schematic diagram. (b) lift-off curve.

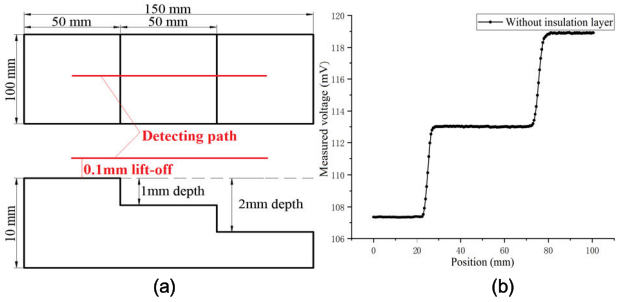

FIGURE 16. The second step of the corrosion depth inversion method: (a) Schematic diagram. (b) The scan curve.

CI sensor (Fig 14) was used to take the measurements with lift-offs increased from 0.1 mm to 5 mm (the red line shown in Fig 15(a)) with a 0.1 mm increment. The lift-off curve which contains 50 points is shown in Fig 15(b). In this case, the vertical axis is measured voltage rather than capacitance. It can be seen that the voltage value from the CI sensor rose monotonously with increased lift-off, which was similar to the trend shown in Fig 8(c).

The second step of the depth inversion is obtaining the scan curve. The CI sensor (shown in Fig 14) was scanned along the scanning path (the red line in Fig 16(a)) at a 0.1 mm lift-off. To eliminate edge effects, the length of the line scan was 100 mm, leaving 25 mm from each end of the specimen. The scan step-size was 0.5 mm. The obtained scan curve (shown in Fig 16(b)) contained 201 points. Again, the measured value in the scan curve can only reflect the step shape, but not the actual depth information.

The fitting inversion was also done with the neural network fitting method. The 50 points lift-off curve (Fig 15(b) was interpolated and the number of points were increased to 491. Another ten-layer neural network was trained with the interpolated lift-off curve, and the scan curve was then taken to the trained neural networks for fitting to obtain the inversion depth (shown in Fig 17). It can be seen from Fig 17 that the inversion depth can reflect the actual depth information, which again proves the effectiveness of the depth inversion method of surface corrosion defects of the conducting specimen without insulation layer.

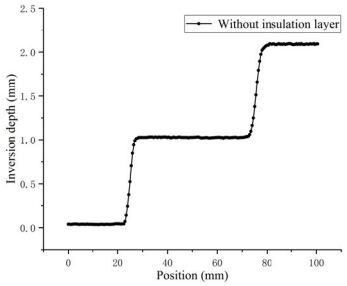

FIGURE 17. Inversion curve for conducting specimen without insulation.

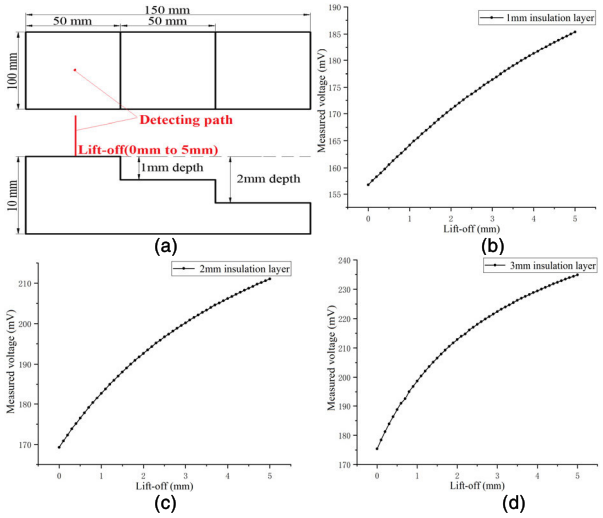

FIGURE 18. The first step of the corrosion depth inversion method: (a) schematic diagram. (b) Lift-off curve with 1 mm insulation layer. (c) Lift-off curve with 2 mm insulation layer. (d) Lift-off curve with 3 mm insulation layer.

B. DEPTH INVERSION FOR SPECIMENS WITH INSULATION LAYERS IN EXPERIMENTS

The same aluminium specimen covered with insulation layers (PMMA) of different thicknesses (1 mm, 2 mm and 3 mm) was inspected. Firstly, an insulation layer with the same thickness of the layer cover on the metal was attached to the CI sensor and the lift-off curve was obtained with lift-offs increased from 0.1 mm to 5 mm (the red line shown in Fig 16(a)) with a 0.1mm increment. 51 point lift-off curves with the CI sensor attached to insulation layers of different thicknesses are shown in Fig 18(b), (c) and (d).

The second step of the depth inversion is obtaining the scan curve. The CI sensor was scanned along the scanning path (the red line in Fig 19(a)) at a 0 mm lift-off. The scan curves with the specimen covered by 1 mm, 2 mm and 3mm insulation layers were obtained and shown in Fig 19(b), (c) and (d).

Three neural networks were trained with the three lift-off curves (after interpolation), and the three scan curves were taken into the corresponding neural network for the depth inversion. The inversion depths are shown in Fig 20 (a), (b) and (c). It can be seen from Fig 20 that the inversion depths can reflect the actual depth information, which proves the effectiveness of the depth inversion method

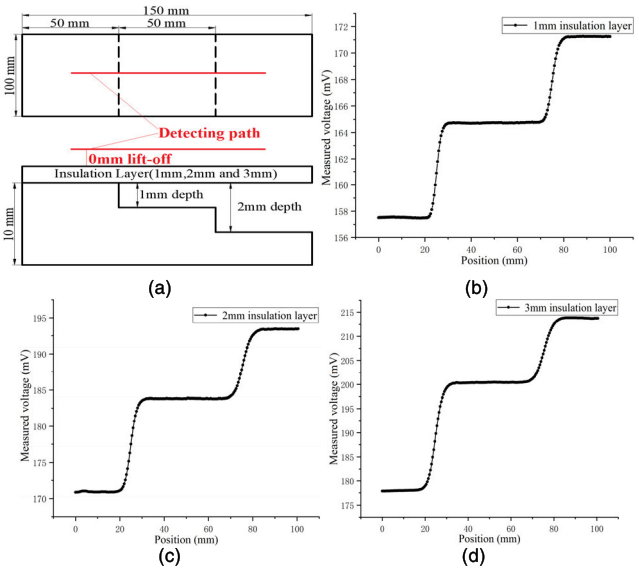

FIGURE 19. The second step of the corrosion depth inversion method: (a) Schematic diagram. (b) Scan curved with 1 mm insulation layer. (c) Experiment results with 2 mm insulation layer. (d) Experiment results with 3 mm insulation layer.

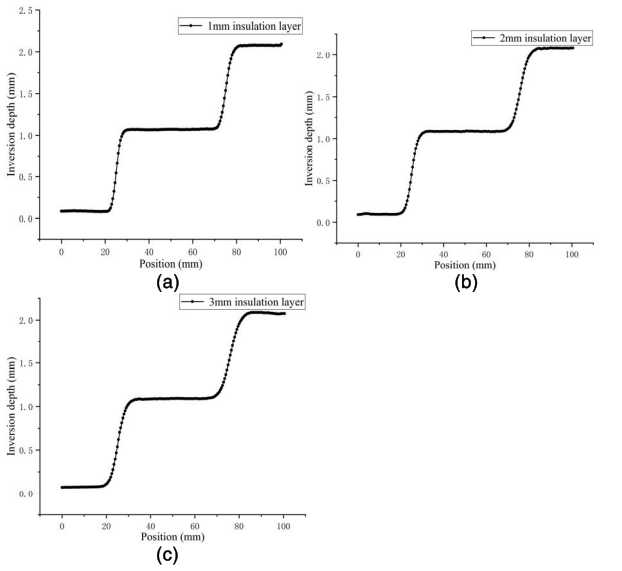

FIGURE 20. Inversion curves: (a) 1 mm insulation layer. (b) 2 mm insulation layer. (c) 3 mm insulation layer.

of surface corrosion defects of the conducting specimen with insulation layer.

The error rates for the depth inversion in experiments (both in Section 4.1 and 4.2) were calculated and shown in Table 2. The errors of the inversion depths were less than 0.1 mm and the error rates of the inversion depths were less than 9.07%. The error rates are higher compared to the ones in FE models due to the influences of experimental conditions (i.e. the control and measurement of lift-offs, humidity and temperature variation, and etc.)

To further illustrate the feasibility of the corrosion depth inversion method in detecting corrosion defects at different depths, experiments on a more practical specimen were

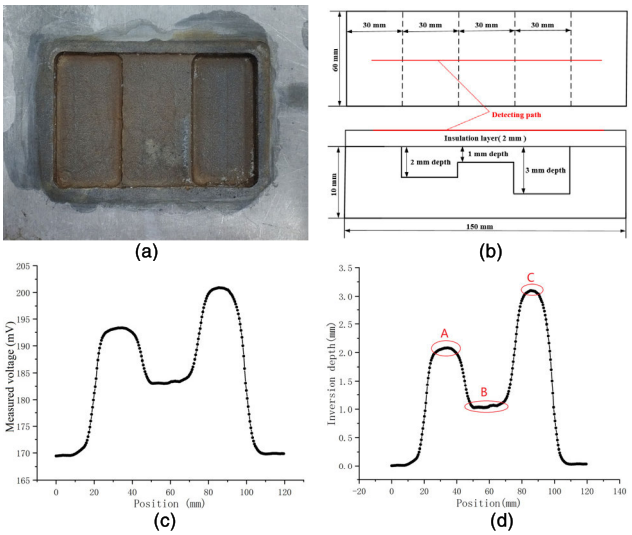

FIGURE 21. Multi-step corrosion detection: (a) Photograph of the machined and corroded specimen. (b) Specifications of the features. (c) The scan curve. (d) The inversion curve.

TABLE 2. Error rates for depth inversion in experiments.

Depth of defect (mm)	Without insulation layer (mm)/ Error rate (%)	1 mm insulation layer (mm) /Error rate (%)	2 mm insulation layer (mm) /Error rate (%)	3 mm insulation layer (mm) /Error rate (%)
1	1.0276/ 2.76	1.0718/ 7.18	1.0853/ 8.53	1.0907/ 9.07
2	2.0924/ 4.62	2.0750/ 3.75	2.0846/ 4.23	2.0730/ 3.65

carried out. As shown in Fig 21(a), a conducting specimen (aluminium plate), which was machined and corroded by ferric chloride, contained three corrosion defects with different depths (2 mm, 1 mm and 3 mm). The dimensions of the features in the specimen are shown in Fig 21 (b). In the experiments, the specimen was covered by a 2 mm insulation layer (PMMA). The scenario is very similar to one case in Section 4.2, and the curve shown in Fig 18 (c) and the trained neural network in section 4.2 can be used for depth inversion. The scan curve for this specimen is shown in Fig 21(c) and the depth inversion result is shown in Fig 21(d). The inversion depths were in good agreement with the corrosion defects of 2 mm, 1 mm and 3 mm, and the error rates were 7.68%, 4.21% and 9.74% respectively.

It can be seen from Fig 21 that, the depth inversion results for the features of different depths, highlighted with red circles labelled "A", "B" and "C", are of different shapes. The inversion curve for the 1 mm deep feature (B) is nearly flat, and the inversion curves for the 2 mm and 3 mm deep features (B and C) are bulges. The bulge is more significant with a deeper feature. This is because the width of the CI sensor is comparable to the width of the targeted features, and the edge effect is more significant. The bulge shape of the inversion curve brings in extra error for depth inversion,

which indicates that the proposed method is more suitable for evaluation corrosion with larger areas compared to the CI sensor. Also, for corrosion of large area but rapid profile change, this method can only be used to estimate the overall severity of the corrosion rather than obtain the exact depth profile.

V. DISCUSSIONS AND CONCLUSIONS

In this paper, a corrosion depth inversion method based on the lift-off effect of the CI technique was introduced. The depth inversion method, which includes establishing lift-off curve, obtaining scan curve and fitting inversion, was implemented in FE models for conducting specimens with and without insulation layers. In the FE models, the errors of the inversion depths were less than 0.002 mm, and the error rates of the inversion depths were less than 1.20%. Depth inversion of surface features on conductors were also carried out in CI experiments for conductor with and without insulation layers. The errors of the inversion depths were less than 0.2 mm, and the error rates of the inversion depths were less than 9.07%. A CI experiments on a machined and corroded specimen further verified the feasibility of the proposed method in evaluating corrosion defects of different depths.

This paper describes a proof-of-concept method for carrion depth inversion using the CI technique. For a clear illustration, significant simplifications were made for both FE modelling and experiments, i.e. uneven corrosions were simulated by flat steps of different depths. It should be noted that, in both FE models and experiments, aluminium specimens were used. However, the conclusions drawn in this paper can be generalised to all kind of highly conducing specimens, i.e. carbon steel, stainless steel and other metal alloys. The reason for that is the probing field from the CI sensor is a quasi-static electric field, and field lines will terminate on (perpendicular to) all kind of conducting surfaces (no matter if the surface is aluminium or steel) and form equipotential surfaces. The limitations of this method was also noticed in the last experiment, the proposed method is more suitable for corrosion with larger areas compared to the CI sensor size. For smaller surface features, an extra parameter, the width of the feature, needs to be considered, in which case a two dimensional data grid for the signal variations of the measured values from two different lift-offs is required. This will be discussed in a separate paper. In future, the robustness of this proposed method on curved objects (i.e. pipes and/or tanks), which requires a lift-off curve on the curved surface will be evaluated. Influencing factors, including thickness and/or material properties of the insulation layer, trade-offs between the sensor size, spatial resolution and thickness of insulation, will be studied.

REFERENCES

[1] D. Xia, "On-line monitoring atmospheric corrosion of metal materials by using a novel corrosion electrochemical sensor," *Corrosion Sci. Protection Technol.*, vol. 29, no. 5, pp. 581–585, 2017.

[2] B. Sasikirono, S. J. Kim, G. D. Haryadi, and A. Huda, "Risk analysis using corrosion rate parameter on gas transmission pipeline," *IOP Conf., Mater. Sci. Eng.*, vol. 202, May 2017, Art. no. 012099, doi: 10.1088/1757-899x/202/1/012099.

[3] A. Afanasyev, A. A. Mel'nikov, S. V. Konovalov, and M. I. Vaskov, "The analysis of the influence of various factors on the development of stress corrosion defects in the main gas pipeline walls in the conditions of the European part of the russian federation," *Int. J. Corrosion*, vol. 2018, pp. 1–10, Jun. 2018, doi: 10.1155/2018/1258379.

[4] N. Nakamura, K. Ashida, T. Takishita, H. Ogi, and M. Hirao, "Inspection of stress corrosion cracking in welded stainless steel pipe using point-focusing electromagnetic-acoustic transducer," *NDT E Int.*, vol. 83, pp. 88–93, Oct. 2016, doi: 10.1016/j.ndteint.2016.06.005.

[5] N. Andruschak, I. Saletes, T. Filleter, and A. Sinclair, "An NDT guided wave technique for the identification of corrosion defects at support locations," *NDT E Int.*, vol. 75, pp. 72–79, Oct. 2015, doi: 10.1016/j.ndteint.2015.06.007.

[6] X. J. Raj and T. Nishimura, "Scanning electrochemical microscopy for the investigation of galvanic corrosion of iron with zinc in 0.1 M NaCl solution," *J. Mater. Eng. Perform.*, vol. 25, no. 2, pp. 474–486, Feb. 2016.

[7] M. Jönsson, B. Rendahl, and I. Annergren, "The use of infrared thermography in the corrosion science area," *Mater. Corrosion*, vol. 61, no. 11, pp. 961–965, Nov. 2010, doi: 10.1002/maco.200905525.

[8] J. Bailey, N. Long, and A. Hunze, "Eddy current testing with giant magnetoresistance (GMR) sensors and a pipe-encircling excitation for evaluation of corrosion under insulation," *Sensors*, vol. 17, no. 10, p. 2229, Sep. 2017, doi: 10.3390/s17102229.

[9] P. Khalili and P. Cawley, "The choice of ultrasonic inspection method for the detection of corrosion at inaccessible locations," *NDT E Int.*, vol. 99, pp. 80–92, Oct. 2018, doi: 10.1016/j.ndteint.2018.06.003.

[10] Y. He, G. Tian, H. Zhang, M. Alamin, A. Simm, and P. Jackson, "Steel corrosion characterization using pulsed eddy current systems," *IEEE Sensors J.*, vol. 12, no. 6, pp. 2113–2120, Jun. 2012, doi: 10.1109/jsen.2012.2184280.

[11] R. Xia, J. Zhou, H. Zhang, L. Liao, R. Zhao, and Z. Zhang, "Quantitative study on corrosion of steel strands based on self-magnetic flux leakage," *Sensors*, vol. 18, no. 5, p. 1396, May 2018, doi: 10.3390/s18051396.

[12] B. Dong, G. Fang, Y. Liu, P. Dong, J. Zhang, F. Xing, and S. Hong, "Monitoring reinforcement corrosion and corrosion-induced cracking by X-ray microcomputed tomography method," *Cement Concrete Res.*, vol. 41, no. 11, pp. 1085–1094, 2011.

[13] M. K. Chang, H. S. Sun, and J. C. Ciou, "Applying ultrasonic testing to detect hole defect near the surface," *Adv. Mater. Res.*, vols. 194–196, pp. 2054–2057, Feb. 2011.

[14] X. Yin, D. A. Hutchins, G. Chen, W. Li, and Z. Xu, "Studies of the factors influencing the imaging performance of the capacitive imaging technique," *NDT E Int.*, vol. 60, pp. 1–10, Dec. 2013, doi: 10.1016/j.ndteint.2013.07.001.

[15] X. Yin, G. G. Diamond, and D. A. Hutchins, "Further investigations into capacitive imaging for NDE," *Insight*, vol. 51, no. 9, pp. 484–490, Sep. 2009, doi: 10.1784/insi.2009.51.9.484.

[16] Z. Li, G. Chen, Y. Gu, K. Wang, W. Li, and X. Yin, "Further investigations into the capacitive imaging technique using a multi-electrode sensor," *Appl. Sci.*, vol. 8, no. 11, p. 2296, Nov. 2018, doi: 10.3390/app8112296.

[17] Z. Li, G. Chen, C. Li, J. Fu, Y. Gu, W. Li, and X. Yin, "Performance evaluation of capacitive imaging sensors with different geometries," *Insight*, vol. 60, no. 12, pp. 676–684, Dec. 2018, doi: 10.1784/insi.2018.60.12.676.

[18] G. Dobie, S. Gareth Pierce, and G. Hayward, "The feasibility of synthetic aperture guided wave imaging to a mobile sensor platform," *NDT E Int.*, vol. 58, pp. 10–17, Sep. 2013, doi: 10.1016/j.ndteint.2013.04.002.

[19] V. Reimund, M. Pelkner, M. Kreutzbruck, and J. Haueisen, "Sensitivity analysis of the non-destructive evaluation of micro-cracks using GMR sensors," *NDT E Int.*, vol. 64, pp. 21–29, Jun. 2014, doi: 10.1016/j.ndteint.2014.02.003.

[20] C. Tholin-Chittenden and M. Soleimani, "Planar array capacitive imaging sensor design optimization," *IEEE Sensors J.*, vol. 17, no. 24, pp. 8059–8071, Dec. 2017, doi: 10.1109/jsen.2017.2719579.

[21] A. D. N. Wrasse, T. P. Vendruscolo, E. N. Santos, F. C. Castaldo, R. E. M. Morales, and M. J. Da Silva, "Capacitive direct-imaging sensor for two-phase flow visualization," in *Proc. IEEE Sensors*, Oct. 2016, pp. 1–3, doi: 10.1109/icsens.2016.7808576.

[22] N. T. Trung and P. Hafliger, "A submicrowatt implantable capacitive sensor system for biomedical applications," *IEEE Trans. Circuits Syst. II, Exp. Briefs*, vol. 62, no. 2, pp. 209–213, Feb. 2015.

XIAOKANG YIN received the B.E. degree in information engineering from the East China University of Science and Technology, Shanghai, China, in June 2005, and the M.S. degree in advanced electronics engineering and the Ph.D. degree in engineering from the University of Warwick, Coventry, U.K., in January 2007 and May 2011, respectively.

He joined the China University of Petroleum, Qingdao, China, in November 2011, where he is currently an Associate Professor with the Department of Mechanical and Electronics Engineering and the Centre for Offshore Engineering and Safety Technology.

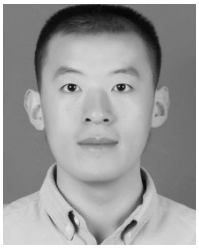

ZHEN LI received the M.E. degree from the China University of Petroleum, Qingdao, China, in 2017, where he is currently pursuing the Ph.D. degree in safety science and engineering with the Center for Offshore Engineering and Safety Technology, Research Institute.

His research interests include nondestructive testing, signal processing, and simulation and inversion imaging. Especially, he does research in capacitive imaging (CI).

XIN'AN YUAN was born in Nanyang, China, in March 1990. He received the B.E. and M.E. degrees in mechanical design manufacture and automation from the China University of Petroleum, Huangdao, China, in 2013 and 2016, respectively, where he is currently pursuing the Ph.D. degree in mechanical engineering with the Center for Offshore Engineering and Safety Technology, Research Institute.

His research interests include nondestructive testing, signal processing, and simulation. Especially, he does research in alternating current measurement field.

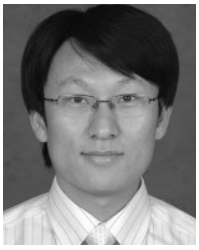

WEI LI (Member, IEEE) received the Ph.D. degree in mechanical and electronics engineering from the China University of Petroleum, Huangdao, China, in 2007.

He joined the China University of Petroleum, where he is currently a Professor of mechanical and electronics engineering. His current research interests include electromagnetic nondestructive evaluation and signal processing, offshore engineering structure design and FEM analysis, and pipeline safety and reliability assessment.

GUOMING CHEN received the B.E. and M.E. degrees in petroleum mechanical engineering and the Ph.D. degree in mechanical design and theory from the China University of Petroleum, Dongying, China, in 1982, 1986, and 1999, respectively.

He is currently the Director of the Centre for Offshore Engineering and Safety Technology, China University of Petroleum, Qingdao, China. He has published more than 350 articles in the offshore oil and gas safety assessment field. His research interests include offshore oil and gas equipment, troubleshooting and reliability assessment, and safety assessment.